Unique Signatures of Topological Phases in Two-Dimensional THz Spectroscopy

Felix Gerken,[1,2] Thore Posske,[1,2] Shaul Mukamel,[3] and Michael Thorwart[1,2]
[1]I. Institut für Theoretische Physik, Universität Hamburg, Notkestraße 9, 22607 Hamburg, Germany
[2]The Hamburg Centre for Ultrafast Imaging, Luruper Chaussee 149, 22761 Hamburg, Germany
[3]Departments of Chemistry and Physics and Astronomy, University of California, Irvine, California 92697-2025, USA

(Received 14 September 2021; revised 12 January 2022; accepted 3 June 2022; published 27 June 2022)

We develop a microscopic theory for the two-dimensional (2D) spectroscopy of one-dimensional topological superconductors. We consider a ring geometry of an archetypal topological superconductor with periodic boundary conditions, bypassing energy-specific differences caused by topologically protected or trivial boundary modes that are hard to distinguish. We show numerically and analytically that the cross-peak structure of the 2D spectra carries unique signatures of the topological phases of the chain. Our work reveals how 2D spectroscopy can identify topological phases in bulk properties.

DOI: 10.1103/PhysRevLett.129.017401

Topological phases of matter have attracted considerable attention following the discovery of topologically nontrivial magnetic and electronic phenomena like the Berezinskii-Kosterlitz-Thouless transition [1–4] and the integer and fractional quantum Hall effect [5,6]. Some topological systems, such as superconducting quantum wires [7], spin liquids [8], and vortices on surfaces of topological superconductors [9] are predicted to host anyons such as spatially isolated Majorana zero-energy boundary modes that are of interest to quantum information processing [10,11]. Despite experimental evidence of zero-energy modes [12], their topological origin remains inconclusive [13]. Experimental techniques that reliably identify one-dimensional (1D) topological superconductors are badly needed. Current approaches detect the localized zero-energy boundary modes, but cannot unambiguously discriminate them against topologically trivial features that appear close to zero energy as well, like Yu-Shiba-Rusinov states [14–18], Kondo peaks [19,20], Andreev bound states [21], and Caroli-de Gennes-Matricon states [22,23]. In 2D electronic systems, dispersive Majorana edge modes have been shown to increase the linear optical conductivity [24].

A versatile advanced tool is nonlinear 2D spectroscopy [25,26] applied in the THz frequency regime to probe electronic excitations in solid-state nanostructures [27–30] or the Fermi glass phase in disordered correlated materials [31]. Recently, 2D spectroscopy of two- and three-dimensional topological spin liquids has theoretically revealed characteristic spectral properties of itinerant spin-based anyons and fractons [32–34] and of strongly correlated two-band Fermi-Hubbard models [35]. It offers additional features in comparison to pump-probe THz spectroscopy [36–39]. The main difference lies in the decoupling of the waiting time and excitation frequency resolution both of which are high [40]. This is in stark contrast to pump-probe spectroscopy where both are inherently connected by a Fourier uncertainty. Moreover, the lack of large background signals permits excellent signal-to-noise ratios.

In this Letter, we employ 2D nonlinear spectroscopy to analyze the periodic Kitaev chain, the archetype of one-dimensional topological superconductors, describing the topological electronic properties of nanowires [12], atomic magnetic chains [41,42], and cold atom systems [43]. Rather than investigating the Majorana boundary modes of this model, we consider a periodic configuration to study the topological properties of the bulk and characterize its two phases by 2D spectroscopy. This could be realized by atomic chain quantum corrals. In particular, we compare Kitaev chains with the same bulk energy spectrum but a different topological phase. We predict experimental signatures due to topological effects, eliminating differences caused solely by the bulk energy spectra or topologically trivial or nontrivial localized zero-energy states. We find signatures of superconducting topological band inversion in the 2D spectra, which are characteristic for the topological phase and which are absent in linear absorption spectra. Our predictions should be verifiable by 2D THz spectroscopy [27–31].

Model.—The Kitaev chain is a 1D spin-polarized unconventional superconductor with the Hamiltonian

$$H = \sum_{n=1}^{N} [-w a_{n+1}^{\dagger} a_n - \mu a_n^{\dagger} a_n + \Delta a_n a_{n+1}] + \text{H.c.}, \quad (1)$$

where a_n is a fermionic annihilation operator, 2μ is the chemical potential, w the nearest-neighbor hopping, and Δ is the complex superconducting gap parameter [7]. In physical systems, the parameters can assume a wide range of energies starting from suspended hybridizing atomic chains or semiconductors where they are of the order of eV

and going down to meV in hybridized Yu-Shiba-Rusinov states [12,44]. However, the superconducting gap is always in the meV range or less. The system has an electronic band gap for $|w| \neq |\mu|$ and $\Delta \neq 0$ [7]. For dominant hopping $|w| > |\mu|$, the open chain, i.e., $a_{N+1} = 0$, has an in-gap mode localized at both ends of the chain. Its energy is exponentially small in the system size. In the large-N limit, this mode decomposes into two spatially isolated Majorana operators [7] whose existence is protected by the electronic energy gap in the bulk. The mode can only disappear by closing the gap. Hence, there are two distinct gapped phases: the topologically trivial phase without and the topologically nontrivial phase with Majorana end modes. Both are characterized by a $\mathbb{Z}_2$ topological invariant of the bulk only [45,46]. The boundary modes are due to an interface between different topological phases explained by the bulk boundary correspondence [47].

Kitaev [7] has already pointed out that there is a map in form of a simple parameter transformation that leaves the band structure of the periodic chain invariant but changes the topological phase. We find that the transformed parameters are given by

$$\mu' = \pm w, \qquad w' = \pm \mu, \qquad \Delta' = e^{i\vartheta}\sqrt{\mu^2 + |\Delta|^2 - w^2}, \tag{2}$$

where ϑ is an arbitrary real number. If the system is originally in the nontrivial phase, i.e., $|\mu| < |w|$, then the transformed chain with the primed parameters will be in the trivial phase, because $|w'| = |\mu| < |w| = |\mu'|$. The same holds vice versa. By this, a dual Hamiltonian with the same spectrum but the inverse topological phase is assigned to each topologically trivial one. Yet, if $\mu^2 + |\Delta|^2 - w^2 < 0$, which can only happen in the nontrivial phase, there will be no trivial Hamiltonian with the same band structure.

We start with the simplest case, $w = \Delta$. The linear transformation U defined by

$$U^\dagger a_n U = i(a_n^\dagger - a_n - a_{n+1}^\dagger - a_{n+1})/2 \tag{3}$$

corresponds to the transformed parameters $\mu' = w$ and $w' = \Delta' = \mu$. In general, we can construct the map between the phases by concatenating the Bogoliubov transformation diagonalizing the trivial Hamiltonian with the inverse of the transformation that diagonalizes the nontrivial Hamiltonian with the same band structure. Even simpler, the map in Eq. (3) can be extended to $|w| \leq |\Delta|$ by fixing the superconducting phase to $\varphi = \arccos(w/|\Delta|)$.

2D spectroscopy.—In 2D spectroscopy, the system is subjected to three consecutive electromagnetic pulses and its response is probed by interference with a fourth pulse [25,26]. In the dipole approximation, i.e., when the shortest wavelength of the light is much larger than the extent of the chain, the radiation-matter interaction Hamiltonian reads $V(t) = -\boldsymbol{d} \cdot \boldsymbol{E}(t)$, where $\boldsymbol{d}$ denotes the dipole operator and $\boldsymbol{E}(t)$ the electric field. For the Kitaev chain, $\boldsymbol{d} = -e\boldsymbol{R}$ with the position operator $\boldsymbol{R} = \sum_{n=1}^{N} \boldsymbol{r}_n a_n^\dagger a_n$ and e the electron charge. Here, $\boldsymbol{r}_n$ is the location of site n. We consider a ring of radius r with $\boldsymbol{r}_n = r(\cos(2\pi n/N), \sin(2\pi n/N), 0)^T$. A similar dipole operator emerges from a low-energy description of realistic systems as shown for a Rashba wire in the Supplemental Material [48].

We are interested in the time-dependent polarization $\boldsymbol{P}(t) = \langle \boldsymbol{d}(t) \rangle_{\rho(t)}$, which provides the measurable electromagnetic response. Here, $\rho(t)$ is the density matrix of matter. Because the system consists of broad electronic bands, we compute the full third-order signal $\boldsymbol{P}^{(3)}(t)$ for the 2D spectra, which is the sum of all phase matching directions. It can be detected in a collinear beam geometry. Breaking it into phase matching components could reveal additional information on specific groups of dynamical pathways, which goes beyond the present study. Coherent 2D techniques, in particular the double quantum coherence, are usually applied to discrete electronic systems like molecules [49].

We assume that at time $t = 0$ the system is in its ground state, and obtain the third-order contribution to the polarization [25,26]

$$P^{(3),j}(t) = \int_0^\infty dt_3 dt_2 dt_1 E^m(t - t_3) E^l(t - t_3 - t_2) \times E^k(t - t_3 - t_2 - t_1) S^{(3),j}_{klm}(t_3, t_2, t_1), \tag{4}$$

with a sum over repeated indices and the third-order response function $S^{(3),j}_{klm}(t_3, t_2, t_1)$. The 2D signal is displayed by its Fourier transform

$$S^{(3),j}_{klm}(\omega_3, t_2, \omega_1) = \frac{2}{\hbar^3}\theta(t_2) \sum_{\alpha=1}^{4} \int_0^\infty \int_0^\infty \mathrm{Im} C^j_{\alpha,klm}(t_3, t_2, t_1) \times e^{i(\omega_1 t_1 + \omega_3 t_3)} dt_1 dt_3, \tag{5}$$

with the Heaviside function $\theta(t)$ and C_α are the four-point correlation functions of the dipole operator (see the Supplemental Material [48]). ω_1 and ω_3 are the excitation and detection frequency, respectively, and t_2 the waiting time. In the following, we set $t_2 = 0$.

Results.—We restrict the discussion to the $S^{(3),x}_{xxx}$ component, where all light pulses are polarized in the x direction. The signals for this feasible configuration are similar to the ones for a physically unrealistic linear chain with periodic boundary conditions. We choose a representative slice in the $(w = \Delta)$ plane to demonstrate the parameter dependence of the 2D spectra. By this, we can use the map in Eq. (3) to clarify the qualitative differences between the phases. Representatives of the two phases are the trivial atomistic limit (dissected atoms) and the sweet spot of the Majorana chain that hosts localized Majorana modes in an open chain. We fix the maximal quasiparticle energy Λ as the energy scale. In our case, Λ can be in the meV regime, but depending on the physical system, Λ can vary up to eV [12,44]. We follow the trajectory

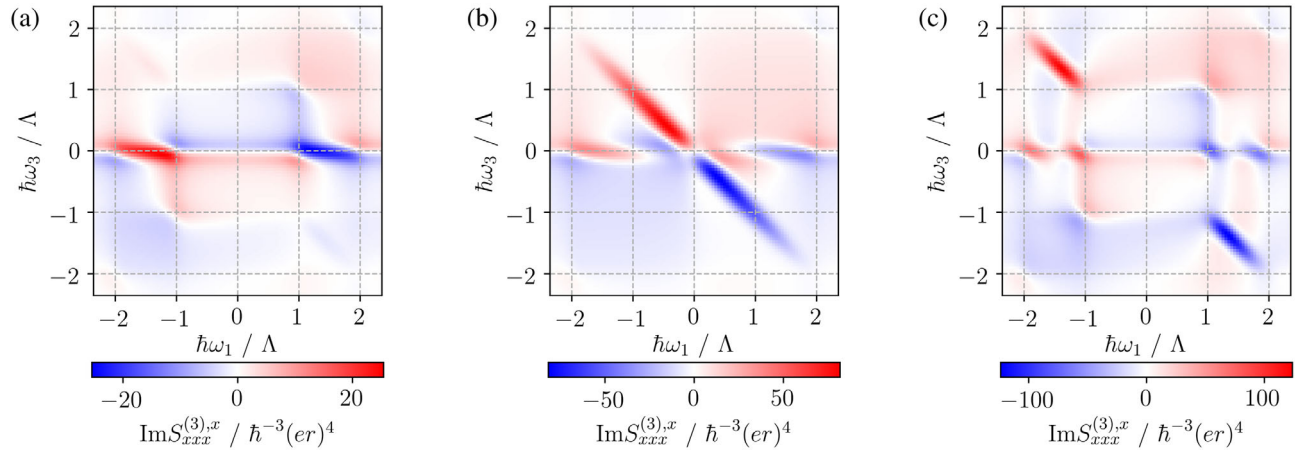

FIG. 1. Imaginary part of the 2D spectrum of the Kitaev ring at waiting time $t_2 = 0$ (a) in the topologically trivial phase with $\mu = 0.375\Lambda, w = \Delta = 0.125\Lambda$, (b) at the critical point in between with $\mu = 0.25\Lambda, w = \Delta = 0.25\Lambda$, and (c) in the nontrivial phase with $\mu = 0.125\Lambda, w = \Delta = 0.375\Lambda$. The chain length is $N = 60$, Λ is the maximal excitation energy of a single quasiparticle. The topologically trivial and nontrivial phases are distinguished by peaks on the counterdiagonal and the splitting of the peak on the horizontal.

$$\Gamma_s = (\mu_s, w_s, \Delta_s) = \Lambda(1 - s, s, s)/2, \tag{6}$$

where $0 \leq s \leq 1$, which interpolates between the two extreme cases $H(\Gamma_0)$ being the Hamiltonian in the atomistic limit and $H(\Gamma_1)$ the Hamiltonian for the sweet spot, such that Λ remains unchanged at all instances. For $s < 0.5$, $H(\Gamma_s)$ is in the topologically trivial phase, for $s > 0.5$ in the nontrivial phase, and for $s = 0.5$, the system reaches the semimetallic critical point, where the bulk gap closes. The spectra and band structures of $H(\Gamma_s)$ and $H(\Gamma_{1-s})$ coincide due to the map U in Eq. (3). By this, 2D spectra for different topological phases with the same eigenenergies can be compared.

Representative 2D spectra for a band gap of $\Lambda/2$ and for the gapless critical point are shown in Fig. 1 (see also the Supplemental Movie [48]). They include a Gaussian broadening ($\sigma = 0.05\Lambda$) to increase readability. Noticeable peaks in the 2D spectra are arranged along three main axes, the diagonal $\omega_1 = \omega_3$, the counterdiagonal $\omega_1 = -\omega_3$, and the horizontal $\omega_3 = 0$. Valuable information is contained in the cross peaks on the counterdiagonal and the horizontal. A change of the cross-peak pattern is observed when passing from the topologically trivial to the nontrivial phase. The counterdiagonal peaks dominate the nontrivial phase, while they almost disappear in the trivial phase. The horizontal peaks appear in both phases. They form a large inhomogeneously broadened peak in the trivial phase but become disconnected in the nontrivial phase and are most pronounced at the band edges. Furthermore, their relative magnitude significantly decreases. In general, the overall magnitude of the 2D spectra increases for $s \to 1$. The peak amplitudes between the phases differ by orders of magnitude. For perfectly flat bands in the trivial phase, they can even vanish due to the charge conserving nature of the dipole operator. The ground state in the trivial phase with flat bands is either the empty or fully filled lattice. There are no other states with the same charge, hence, all transitions are forbidden. For flat bands in the nontrivial phase, there are numerous possible transitions, in contrast. The charge expectation value of the ground state is $-Ne/2$. We estimate

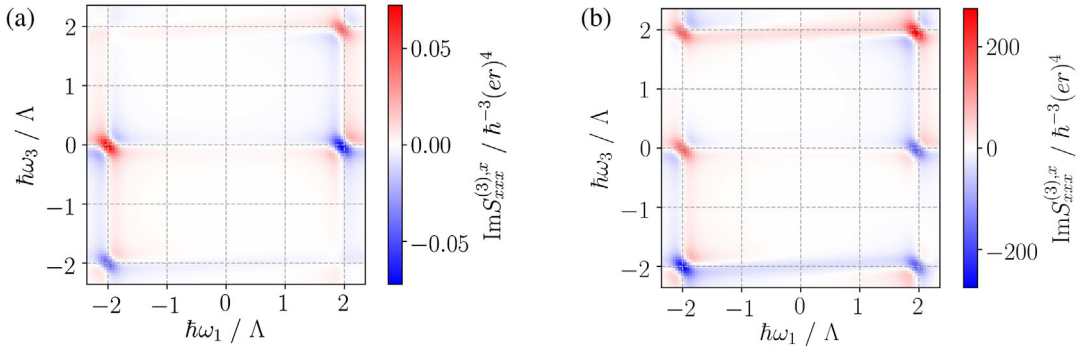

FIG. 2. Imaginary part of the 2D spectrum of the Kitaev ring in (a) the topologically trivial phase with $\mu = 0.005\Lambda, w = \Delta = 0.495\Lambda$, and (b) the nontrivial phase with $\mu = 0.495\Lambda$ and $w = \Delta = 0.005\Lambda$ for $N = 60$.

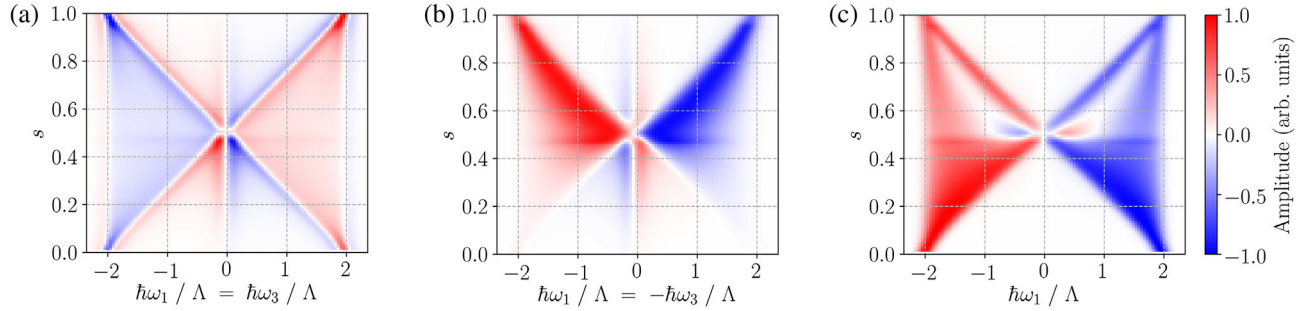

FIG. 3. (a) Diagonal, (b) counterdiagonal, and (c) horizontal sections of the imaginary part of the 2D spectra for the Hamiltonian $H(\Gamma_s)$ as a function of s following Eq. (6). For each parameter set Γ_s, the 2D spectra are normalized to their maximal peak amplitude. The chain length is $N = 60$. Differences between the topological phases emerge along the counterdiagonal and the horizontal lines. In the trivial phase ($s < 0.5$), the counterdiagonal peaks disappear. The horizontal peaks are more pronounced in the trivial phase than in the nontrivial phase ($s > 0.5$).

that for even N, the number of Fock states with charge $-Ne/2$ is $2^N/\sqrt{N}$ due to Sterling's formula. This accounts for the discrepancy of the magnitudes between the 2D spectra of the almost flat band scenarios shown in Fig. 2.

For the nearly flat bands in Fig. 2, we find essential differences between the 2D spectra of the two topological phases. In the trivial phase, the horizontal peaks are the dominant cross peaks while counterdiagonal peaks are absent. In the nontrivial phase, the counterdiagonal peaks are dominant while the horizontal peaks are reduced. To show that this is generic, we depict the cross sections along the diagonal, counterdiagonal, and horizontal in Fig. 3. For each value of s, the 2D spectra are normalized to their maximal peak amplitude. The diagonal at $t_2 = 0$ carries information on the linear response spectra. We find the 2D spectra to be symmetric about the phase transition at $s = 0.5$. This reaffirms that the linear response cannot uncover differences between the phases. Our analytic calculations show that the difference between the phases in linear spectroscopy is essentially a scaling factor [48]. For the counterdiagonal, cross peaks disappear in the trivial regime $s < 0.5$, but are strong in the nontrivial regime $s > 0.5$. Importantly, the change in the relative peak amplitudes when crossing the critical point $s = 0.5$ is continuous. The signal from the horizontal sections forms a broad continuum in the trivial phase that is clearly split in the topological phase. This is caused by the superconducting topological band inversion characteristic for the model. The anomalous term in Eq. (1) mixes the particle and hole bands. In the trivial phase, the bands maintain their predominant particle and hole character, respectively. In the topological phase, the bands change between particle and hole character at the inversion points in the Brillouin zone. There, the nonvanishing two-particle to two-particle transition dipole moments have a gap closure [48]. This is absent in the trivial phase and is thus unique to the topological phase. For large N, their transition frequencies go to zero. Hence, they contribute to the horizontal peaks in the 2D spectra, and the observed splitting of the peak continua provides a clear signature of the superconducting topological band inversion. The difference in the cross peaks and the absence of any difference in the diagonal peaks are a fundamental advantage of nonlinear spectroscopy for characterizing topological phases. Our results transfer to finite Kitaev chains with open boundary conditions. Yet, additional Majorana end modes as well as possible trivial zero-energy modes result in a doubling of the 2D spectrum at energies of the order of the band gap that must be accounted for. Remarkably, the bulk contribution is qualitatively the same as for the periodic configuration, suggesting that our results are largely insensitive to the specific geometry underlying the dipole operator. Furthermore, local parametric disorder of up to 30% of the band gap energy does not significantly affect the signature of the topological phase. These two observations suggest the robustness of the signature of the topological phase (see the Supplemental Material [48] for more details).

The map U offers an alternative interpretation of our results. Rather than considering U to actively change the topological phase, we could equivalently consider the Hamiltonian to be invariant and passively transform the measurement operator, i.e., the dipole operator, which has the form of a local chemical potential, into the Majorana braiding operator $B_{n,n+1} = a^\dagger_{n+1}a_n + a_{n+1}a_n + \text{H.c.}$ for adjacent sites [50]. Formally, this means $U^\dagger \boldsymbol{d} U = (e/2)\sum_{n=1}^{N} \boldsymbol{r}_n B_{n,n+1}$. Then, the 2D spectrum can be interpreted in two ways: first, the chain being in one phase and probed by the common dipole operator, and second the chain being in the other phase and probed by the braiding operator.

Conclusions.—With the Kitaev ring, we propose a physical realization of the Kitaev chain with periodic boundary conditions and calculate the THz response in 2D nonlinear spectroscopy with three parallel polarized field pulses. By a mapping between the topologically trivial and nontrivial phases that changes the phase but not the band structure of the Kitaev Hamiltonian, we identify signatures stemming solely from topological effects and

not from the energy spectra. A superconducting topological band inversion is then detected by cross peaks in the 2D spectra, which underlines the advantage of nonlinear spectroscopy over linear spectroscopy for topological systems. A band inversion has recently been resolved in scanning tunneling microscope experiments [44], which couples to the local charge rather than the dipole operator. 2D spectroscopy is less invasive, offers higher spectral resolution, and is less prone to dissipation, where any backaction of a macroscopic tip on the quantum system can be excluded. A seeming caveat of our approach is that the superconducting gap Δ should be rather large for the U map to exist. However, our analytic computation of the dipole moments [48] suggests that our results carry over to small Δ. In contrast to topological spin liquids [32,33], the electronic system at hand can be probed both in its topologically trivial and nontrivial phase, and its topological features are revealed by bulk properties only, omitting the spectroscopy of hard-to-control low-energy topological quasiparticles that interfere with the topological response of the bulk. Future research on multiple topological band inversions and multiband models could help to establish a general connection between our findings and the bulk topological invariant.

We thank Hong-Guang Duan for helpful discussions. M. T. and F. G. acknowledge support by the Cluster of Excellence "CUI: Advanced Imaging of Matter" of the Deutsche Forschungsgemeinschaft (DFG)—EXC 2056—project ID 390715994. T. P. acknowledges funding by the Deutsche Forschungsgemeinschaft (DFG) project no. 420120155. S. M. gratefully acknowledges the support of the National Science Foundation Grant CHE-1953045.

[1] V. L. Berezinskii, Sov. Phys. JETP **32**, 493 (1971), http://www.jetp.ras.ru/cgi-bin/e/index/e/32/3/p493?a=list.
[2] V. L. Berezinskii, Sov. Phys. JETP **34**, 610 (1972), http://www.jetp.ras.ru/cgi-bin/e/index/e/34/3/p610?a=list.
[3] J. M. Kosterlitz and D. J. Thouless, J. Phys. C **5**, L124 (1972).
[4] J. M. Kosterlitz and D. J. Thouless, J. Phys. C **6**, 1181 (1973).
[5] K. v. Klitzing, G. Dorda, and M. Pepper, Phys. Rev. Lett. **45**, 494 (1980).
[6] D. C. Tsui, H. L. Störmer, and A. C. Gossard, Phys. Rev. Lett. **48**, 1559 (1982).
[7] A. Kitaev, Phys. Usp. **44**, 131 (2001).
[8] A. Kitaev, Ann. Phys. (Amsterdam) **321**, 2 (2006).
[9] L. Fu and C. L. Kane, Phys. Rev. Lett. **100**, 096407 (2008).
[10] C. Nayak, S. H. Simon, A. Stern, M. Freedman, and S. Das Sarma, Rev. Mod. Phys. **80**, 1083 (2008).
[11] J. Alicea, Y. Oreg, G. Refael, F. von Oppen, and M. P. A. Fisher, Nat. Phys. **7**, 412 (2011).
[12] V. Mourik, K. Zuo, S. M. Frolov, S. R. Plissard, E. P. A. M. Bakkers, and L. P. Kouwenhoven, Science **336**, 1003 (2012).
[13] H. Zhang *et al.*, Nature (London) **591**, E30 (2021).
[14] L. Yu, Acta Phys. Sin. **114**, 75 (1965).
[15] H. Shiba, Prog. Theor. Phys. **40**, 435 (1968).
[16] A. I. Rusinov, JETP Lett. **9**, 85 (1969), http://jetpletters.ru/ps/1658/article_25295.shtml.
[17] B. W. Heinrich, J. I. Pascual, and K. J. Franke, Prog. Surf. Sci. **93**, 1 (2018).
[18] L. Cornils, A. Kamlapure, L. Zhou, S. Pradhan, A. A. Khajetoorians, J. Fransson, J. Wiebe, and R. Wiesendanger, Phys. Rev. Lett. **119**, 197002 (2017).
[19] E. Müller-Hartmann and J. Zittartz, Phys. Rev. Lett. **26**, 428 (1971).
[20] C. P. Moca, I. Weymann, M. A. Werner, and G. Zaránd, Phys. Rev. Lett. **127**, 186804 (2021).
[21] P. Yu, J. Chen, M. Gomanko, G. Badawy, E. P. A. M. Bakkers, K. Zuo, V. Mourik, and S. M. Frolov, Nat. Phys. **17**, 482 (2021).
[22] C. Caroli, P. de Gennes, and J. Matricon, Phys. Lett. **9**, 307 (1964).
[23] D. Wang, L. Kong, P. Fan, H. Chen, S. Zhu, W. Liu, L. Cao, Y. Sun, S. Du, J. Schneeloch, R. Zhong, G. Gu, L. Fu, H. Ding, and H.-J. Gao, Science **362**, 333 (2018).
[24] J. J. He, Y. Tanaka, and N. Nagaosa, Phys. Rev. Lett. **126**, 237002 (2021).
[25] S. Mukamel, *Principles of Nonlinear Optics and Spectroscopy* (Oxford University Press, New York, 1995).
[26] L. Valkunas, D. Abramavicius, and T. Mančal, *Molecular Excitation Dynamics and Relaxation* (Wiley-VCH, Weinheim, 2013).
[27] W. Kuehn, K. Reimann, M. Woerner, T. Elsaesser, and R. Hey, J. Phys. Chem. B **115**, 5448 (2011).
[28] M. Woerner, W. Kuehn, P. Bowlan, K. Reimann, and T. Elsaesser, New J. Phys. **15**, 025039 (2013).
[29] G. Nardin, Semicond. Sci. Technol. **31**, 023001 (2016).
[30] S. Markmann, M. Franckié, S. Pal, D. Stark, M. Beck, M. Fiebig, G. Scalari, and J. Faist, Nanophotonics **10**, 171 (2021).
[31] F. Mahmood, D. Chaudhuri, S. Gopalakrishnan, R. Nandkishore, and N. P. Armitage, Nat. Phys. **17**, 627 (2021).
[32] W. Choi, K. H. Lee, and Y. B. Kim, Phys. Rev. Lett. **124**, 117205 (2020).
[33] R. M. Nandkishore, W. Choi, and Y. B. Kim, Phys. Rev. Research **3**, 013254 (2021).
[34] Y. Wan and N. P. Armitage, Phys. Rev. Lett. **122**, 257401 (2019).
[35] N. T. Phuc and P. Q. Trung, Phys. Rev. B **104**, 115105 (2021).
[36] T. Elsaesser, K. Reimann, and M. Woerner, *Concepts and Applications of Nonlinear Terahertz Spectroscopy* (Morgan & Claypool Publishers, San Rafael, 2019).
[37] J. Lu, X. Li, Y. Zhang, H. Y. Hwang, B. K. Ofori-Okai, and K. A. Nelson, Top. Curr. Chem. **376**, 6 (2018).
[38] R. Ulbricht, E. Hendry, J. Shan, T. F. Heinz, and M. Bonn, Rev. Mod. Phys. **83**, 543 (2011).
[39] S.-H. Shima and M. T. Zanni, Phys. Chem. Chem. Phys. **11**, 748 (2009).
[40] A. Gelzinis, R. Augulis, V. Butkus, B. Robert, and L. Valkunas, Biochim. Biophys. Acta **1860**, 271 (2019).
[41] S. Nadj-Perge, I. K. Drozdov, J. Li, H. Chen, S. Jeon, J. Seo, A. H. MacDonald, B. A. Bernevig, and A. Yazdani, Science **346**, 602 (2014).

[42] H. Kim, A. Palacio-Morales, T. Posske, L. Rózsa, K. Palotás, L. Szunyogh, M. Thorwart, and R. Wiesendanger, Sci. Adv. **4**, eaar5251 (2018).
[43] J. Ruhman, E. Berg, and E. Altman, Phys. Rev. Lett. **114**, 100401 (2015).
[44] L. Schneider, P. Beck, T. Posske, D. Crawford, E. Mascot, S. Rachel, R. Wiesendanger, and J. Wiebe, Nat. Phys. **17**, 943 (2021).
[45] A. Kitaev, AIP Conf. Proc. **1134**, 22 (2009).
[46] Note that the Kitaev chain possesses an artificial time-reversal symmetry and is therefore in the Cartan-Altland-Zirnbauer class BDI with a $\mathbb{Z}$ invariant. However, this symmetry is broken by realistic perturbations. Hence, we consider the system to be in class D.
[47] A. M. Essin and V. Gurarie, Phys. Rev. B **84**, 125132 (2011).
[48] See Supplemental Material at http://link.aps.org/supplemental/10.1103/PhysRevLett.129.017401 for further details and Supplemental Movie 1 for the 2D spectra as the system parameters vary. The spectra in the movie are normalized to the maximal peak amplitude for each set of parameters.
[49] D. Abramavicius, B. Palmieri, D. V. Voronine, F. Šanda, and S. Mukamel, Chem. Rev. **109**, 2350 (2009).
[50] D. A. Ivanov, Phys. Rev. Lett. **86**, 268 (2001).